Probing Intracellular Biomarkers and Mediators of Cell Activation Using Nanosensors and Bioorthogonal Chemistry

Jered B. Haun,[†] Neal K. Devaraj,[†] Brett S. Marinelli,[†] Hakho Lee,[†] and Ralph Weissleder[†,‡,*]

[†]Center for Systems Biology, Massachusetts General Hospital, 185 Cambridge Street, CPZN 5206, Boston, Massachusetts 02114, United States and [‡]Department of Systems Biology, Harvard Medical School, 200 Longwood Avenue, Boston, Massachusetts 02115, United States

ABSTRACT Nanomaterials offer unique physical properties that make them ideal biosensors for scant cell populations. However, specific targeting of nanoparticles to intracellular proteins has been challenging. Here, we describe a technique to improve intracellular biomarker sensing using nanoparticles that is based on bioorthogonal chemistry. Using *trans*-cyclooctene-modified affinity ligands that are administered to semipermeabilized cells and revealed by cycloaddition reaction with tetrazine-conjugated nanoparticles, we demonstrate site-specific amplification of nanomaterial binding. We also show that this technique is capable of sensing protein biomarkers and phosphoprotein signal mediators, both within the cytosol and nucleus, *via* magnetic or fluorescent modalities. We expect the described method will have broad applications in nanomaterial-based diagnostics and therapeutics.

KEYWORDS: nanoparticles · intracellular · targeting · bioorthogonal chemistry · tetrazine · diagnostic magnetic resonance · cancer

Human cells, and in particular cancer cells, exhibit substantial molecular heterogeneity, and it is increasingly apparent that methods to detect numerous key targets in size-limited clinical samples will become essential to assess the spatial and temporal status of signal transduction networks and to realize the goal of personalized medicine.[1−4] Traditional molecular detection methods such as Western blotting, flow cytometry, immunofluorescence imaging, and immunohistochemistry require prohibitively large cell numbers for these tasks, lack multiplexing capability, or suffer from low throughput, and thus are limited in the amount of information that can be obtained from clinical specimen. Nanomaterial-based detection platforms can provide advantages over these approaches in terms of the signal sensitivity, stability, and/or capability for multiplexing that are afforded by unique physical properties such as paramagnetism,[5,6] semiconductor fluorescence,[7−9] luminescence/fluorescence upconversion,[10,11] or plasmon resonance/Raman scattering.[12] For these reasons, there has been substantial interest in developing sensitive and robust methods to detect biomarkers on the surface of cells or tissues using nanomaterials functionalized with targeting ligands such as monoclonal antibodies.[6,13−21] To date, however, nanomaterial-based detection of biomarkers within cells has been limited to a few studies,[22−26] most likely due to difficulties in achieving sufficient target-to-background ratios. Hence, novel techniques are required to significantly improve the delivery of nanomaterials to intracellular compartments and their ability to specifically recognize targets upon arrival, while also limiting nonspecific interactions. While extensive work has been performed to characterize intracellular uptake and endosomal escape of nanomaterials,[27−29] most sensing applications will require cell permeabilization because delivery into the cytoplasm and nucleus of live cells is inefficient even when cell-penetrating mediators such as the HIV tat peptide are used.[30−32] Advances in nanomaterial delivery and targeting remain a critical need for nanomaterial-based diagnostic applications because key biomarkers and indicators of activation, growth, and survival are located within cells (these potential targets are schematically represented in Figure 1a).

We have recently used bioorthogonal cycloaddition chemistries to target nanoparticle sensors to surface markers such as HER2 and EGFR on live cells.[13,33] This technique, termed bioorthogonal nanoparticle detection (BOND), utilizes an irreversible inverse Diels−Alder reaction between tetrazine (Tz) and a strained dienophile such as norbornene[33,34] or *trans*-cyclooctene (TCO) to couple nanoparticles to affinity molecules pretargeted to the cell surface (Figure 1b).[13,35]

* Address correspondence to rweissleder@mgh.harvard.edu.

Received for review January 26, 2011 and accepted February 25, 2011.

Published online February 25, 2011
10.1021/nn200333m

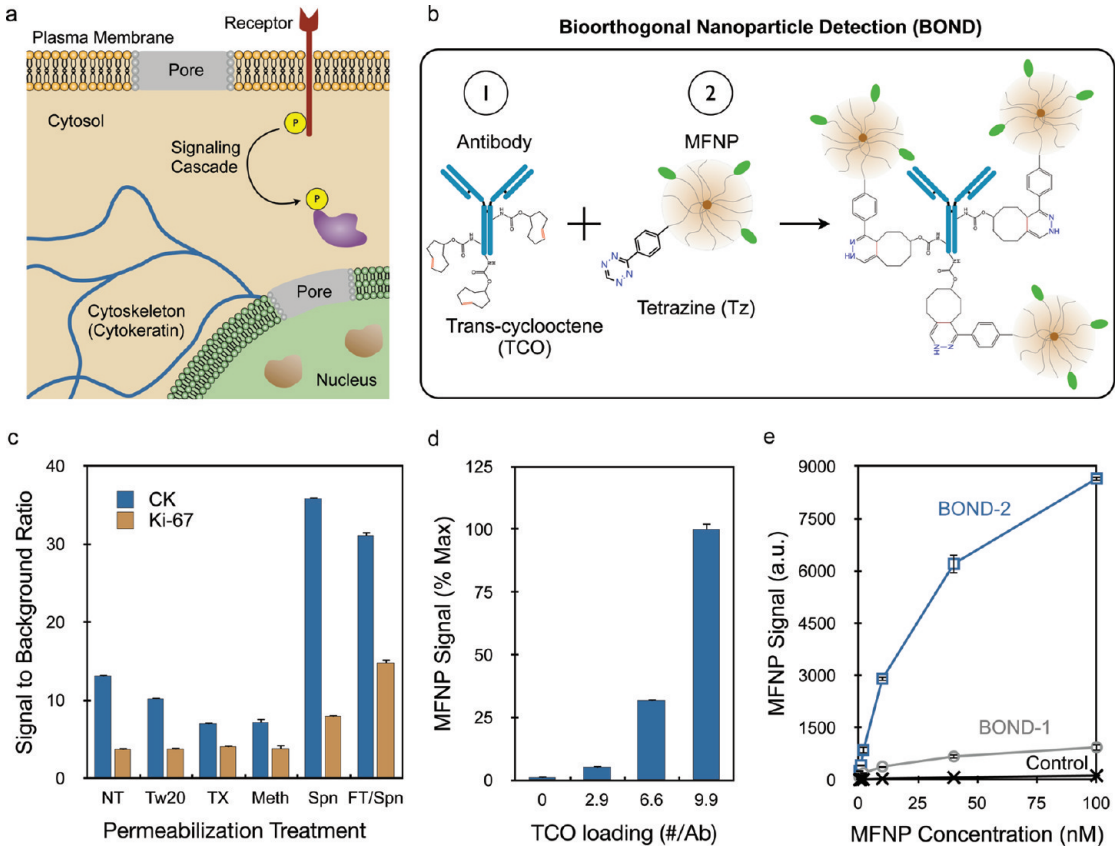

Figure 1. Targeting nanoparticles to intracellular markers using bioorthogonal chemistry coupling. (a) Semipermeabilization of intact cells allows nanoparticle targeting to a variety of intracellular biomarkers as wells as indicators of cell growth, activation, and survival. (b) BOND targeting scheme using a TCO-modified antibody followed by Tz nanoparticle to amplify nanoparticle binding. (c) Investigation of various cell treatments to optimize secondary permeabilization (NT, no treatment; Tw20, Tween 20; TX, Triton X-100; Meth, methanol; Spn, saponin) following fixation. A freeze−thaw treatment prior to fixation was also tested along with saponin (FT/Spn). Optimal MFNP signal-to-background ratios were obtained with the freeze−thaw/Spn treatment for both cytoplasmic (CK) and nuclear (K_i-67) targets. (d) Increasing the TCO valency on the anti-CK antibody increased MFNP signal. (e) Binding isotherms obtained for targeting CK using BOND-2 and a direct MFNP immunoconjugate prepared using the TCO/Tz chemistry (BOND-1). Control signals were obtained using Tz-MFNP only. BOND-2 yielded higher MFNP signals at all concentrations, with differences exceeding 10-fold. Error bars represent the standard error from at least three independent experiments.

Using TCO-modified monoclonal antibodies and Tz nanoparticles, we have shown that this two-step BOND scheme (BOND-2) is specific, rapid, modular, and yields superior nanoparticle signals relative to traditional direct affinity molecule−nanoparticle conjugates due to amplification of binding.[13] This amplification is similar to that observed with other two-step procedures such as primary/secondary antibodies and avidin/biotin, but the small size of the bioorthogonal reagents allows for a significantly higher degree of coupling. Recent evidence suggests that the Tz-TCO chemistry is compatible within the intracellular compartment;[36] however, BOND amplification has not yet been demonstrated inside cells. Therefore, we adapted the technique to the detection of intracellular proteins for rapid and sensitive diagnostic applications.

Here, we significantly improve the sensitivity of intracellular nanomaterial diagnostics by (1) systematically screening cell fixation and permeabilization treatments to optimize nanomaterial delivery and binding specificity and (2) amplifying nanomaterial binding using the bioorthogonal coupling scheme. We demonstrate that different intracellular protein biomarkers (cytosolic, nuclear, phosphorylation specific, *etc.*) can be sensed with unprecedented sensitivity and specificity using magnetic or fluorescent tetrazine nanoparticles. We expect the techniques described will have broad applications in nanomaterial-based diagnostics by enabling detection of cells based on internal biomarkers and longitudinal monitoring of cell status in small and unique populations under numerous modalities.

RESULTS

Optimizing Nanoparticle Delivery and Targeting. We first screened cell fixation and permeabilization treatments to optimize the delivery of nanoparticles to subcellular targets while limiting nonspecific background. Cancer cells were treated in suspension to replicate conditions commonly encountered in clinical diagnostic applications (fine needle aspirates, blood samples for circulating

tumor cells, or other fluid samples) and to facilitate quantification of fluorescence for magneto-fluorescent nanoparticles (MFNP) by flow cytometry. We identified several methods to fix and permeabilize cells from the literature, and a prescreen indicated that the best signal-to-background ratio was obtained using a mixture of formaldehyde and the detergent saponin. Using a cytoplasmic (cytokeratin, CK) and nuclear (K_i-67) protein marker as model diagnostic targets, we then tested the effect of secondary permeabilization treatment with methanol or one of several detergents (Tween 20, Triton-X 100, or additional saponin). MFNP were targeted to CK and K_i-67 using the BOND-2 scheme, employing successive incubations with TCO-modified monoclonal antibody (anti-CK, 9.9 TCO/antibody; anti-K_i-67, 24.4 TCO/antibody) and Tz-MFNP. TCO loadings were determined by matrix-assisted laser desorption/ionization time-of-flight (MALDI-TOF) mass spectrometry (see Supporting Information and Figure S1). Figure 1c summarizes the signal-to-background ratio for each secondary permeabilization treatment and shows that saponin was optimal for both markers. We also investigated whether the results for saponin could be improved by mechanical disruption *via* freeze−thaw treatment prior to fixation. While the cytosolic CK signal was unaffected, a significant increase in nuclear K_i-67 signal was observed along with a small increase in background binding. The combination of the freeze−thaw and saponin treatments thus yielded the best general results and was used for subsequent experiments unless indicated.

We next optimized BOND-2 and compared the technique to direct immuno-conjugation using CK as the target. We first studied the effect of TCO loading on nanoparticle binding (Figure 1d) and found that Tz-MFNP signal increased with TCO valency. This observation was observed previously for targeting extracellular markers where saturation occurred at ~20 TCO/antibody.[13] Such extensive TCO loading was not achieved here for the anti-CK antibody despite similar treatment with amine-reactive TCO, most likely due to decreased number or availability of primary amine modification sites. Figure 1e compares nanoparticle binding as a function of concentration for BOND-2 and an immuno-conjugate that was synthesized using TCO-antibody and Tz-MFNP prior to exposure to cells (BOND-1). We found that the signal for both cases increased out to 100 nM Tz-MFNP concentration, but the two-step procedure yielded approximately an order of magnitude higher signal. Similar results were also obtained for targeting the cytoskeletal protein vimentin (Supporting Information Figure S2). These findings confirm that the BOND-2 scheme amplifies nanoparticle binding to intracellular targets. It is also possible that the smaller size of the Tz nanoparticle (28.8 nm) relative to the immuno-conjugate (41.8 for the anti-CK antibody-MFNP) could provide an advantage with respect to delivery into the cell. For instance, diffusive transport rate scales inversely with size, and thus would be 33% faster for the Tz-MFNP. These data thus demonstrate that the Tz/TCO cycloaddition is compatible with detection of targets inside of cells, and the two-step BOND scheme leads to an order of magnitude higher signal.

Intracellular Nanoparticle Binding Correlates with Target Expression. For diagnostic purposes, it is often important to not only detect the presence or absence of a protein but also to quantitate the amount per cell. We therefore determined whether nanoparticle binding correlated with target protein expression by employing panels of cell lines varying in expression of CK and K_i-67. The CK panel included negative (U118), low (SK-OV-3), moderate (HeLa), and high (SK-BR-3 and PANC-1) expressing cell lines. The K_i-67 panel included cell populations exhibiting low (SK-OV-3 and SK-BR-3), moderate (A549 and HT-29), and high (PANC-1) percentages of actively growing cells. Nanoparticles were targeted using the optimized conditions determined in the previous section (9.9 TCO/anti-CK antibody, 24.4 TCO/anti-K_i-67 antibody, 100 nM Tz-MFNP), and fluorescence intensities were measured using flow cytometry. We found that the nanoparticle signals for both markers correlated closely with expression levels determined by fluorescent antibody staining (Figure 2a) and Western blot (see Supporting Information and Figure S2). Note that nanoparticle binding to the CK negative cell line was identical to the controls, suggesting that background binding is independent of the TCO-antibody. As a final confirmation of nanoparticle binding specificity and to assess the spatial distribution of targeted nanoparticles within cells, we performed confocal microscopy (Figure 2b). For these experiments, we modified the anti-CK and anti-K_i-67 antibodies with both TCO and AlexaFluor-488 (AF488) fluorescent dye to compare localization of antibody and MFNP (conjugated with VT680 near-infrared fluorescent dye). Following separate incubations of fixed/permeabilized SK-BR-3 cells with TCO/AF488-modified anti-CK antibody and Tz-MFNP, strong antibody signal was detected in a manner consistent with cytoskeletal (intermediate filament) structures (Figure 2b,i). Likewise, strong antibody signal was detected exclusively within the nucleus for PANC-1 cells using the TCO/AF488-modified anti-K_i-67 antibody (Figure 2b,v). The corresponding MFNP signals were also bright (Figure 2b,ii,vi) and showed excellent correlation with the antibody signals (Figure 2b,iii,vii). However, no nanoparticle signal was observed when a TCO-modified control antibody was employed (Figure 2b,iv,viii). Similar results were obtained targeting vimentin and p53 (Supporting Information Figure S2). These findings confirm that the Tz/TCO cycloaddition is chemoselective, leading to nanoparticle accumulation at the sites

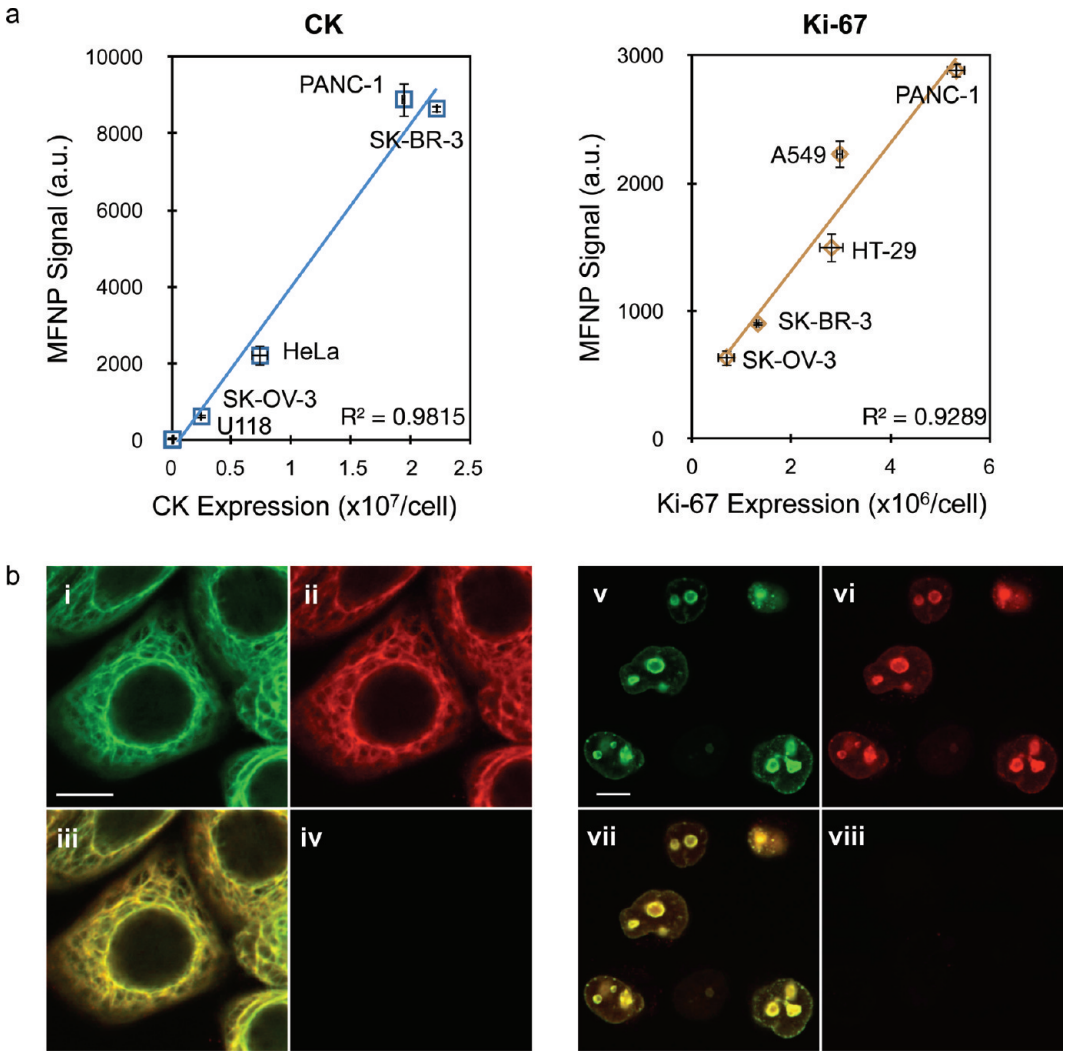

Figure 2. Nanoparticle targeting to intracellular markers is specific and representative of molecular expression level. (a) MFNP fluorescence correlated closely with molecular expression determined by antibody staining for panels of cell lines expressing various amounts of CK and K_i-67. (b) Confocal microscopy images of SK-BR-3 (i−iv) and PANC-1 (v−viii) cells targeted for CK and K_i-67, respectively. In both cases, antibodies were labeled with both TCO (3−4 per antibody) and AlexaFluor-488 fluorescent dye. Following MFNP labeling, images were captured at 488 (antibody, pseudocolored green, i and v) and 680 (MFNP, pseudocolored red, ii and vi) nm emission. Merged images reveal excellent correlation between the two signals (iii and vii). Controls determined using a nonbinding, TCO-modified control antibody were negative (iv and viii). The scale bars in (i) and (v) represent 10 μm. Error bars represent the standard error from at least three independent experiments.

of antibody binding, and thereby molecular target expression.

NMR Profiling of Intracellular Proteins with Magnetic Nanoparticles. We next set out to determine the feasibility of profiling different intracellular proteins based on magnetic resonance effects induced by magnetic nanoparticles. Since biological samples exhibit low endogenous magnetic background, detection of magnetic nanoparticles can be performed in optically obscure (*i.e.*, crude) samples, and as such, diagnostic magnetic resonance (DMR) has received considerable attention for rapid, point-of-care detection of diagnostic specimen containing scant cell populations.[14] These scant cell populations, typically encountered in diagnostic cancer specimen obtained from fine-needle aspirate biopsies or circulating tumor cells (CTCs) from blood, are difficult to quickly and accurately profile using conventional molecular detection methods (*i.e.*, Western blot, immunohistochemistry, flow cytometry). Figure 3a displays the DMR results obtained for eight different cell lines that were profiled for eight intracellular biomarkers relevant to cancer screening (CK, vimentin, K_i-67, and p53) and therapeutic monitoring (cytoplasmic domain of EGFR, phosphorylated EGFR (p-EGFR), phosphorylated ERK (p-ERK), and phosphorylated S6 ribosomal protein (p-S6RP)). In each case, cells were labeled with MFNP using the BOND scheme, and 1000 cells were analyzed in the 1 μL sample volume of a hand-held NMR device. Note the excellent correlation coefficients indicated in Figure 3b between magnetic

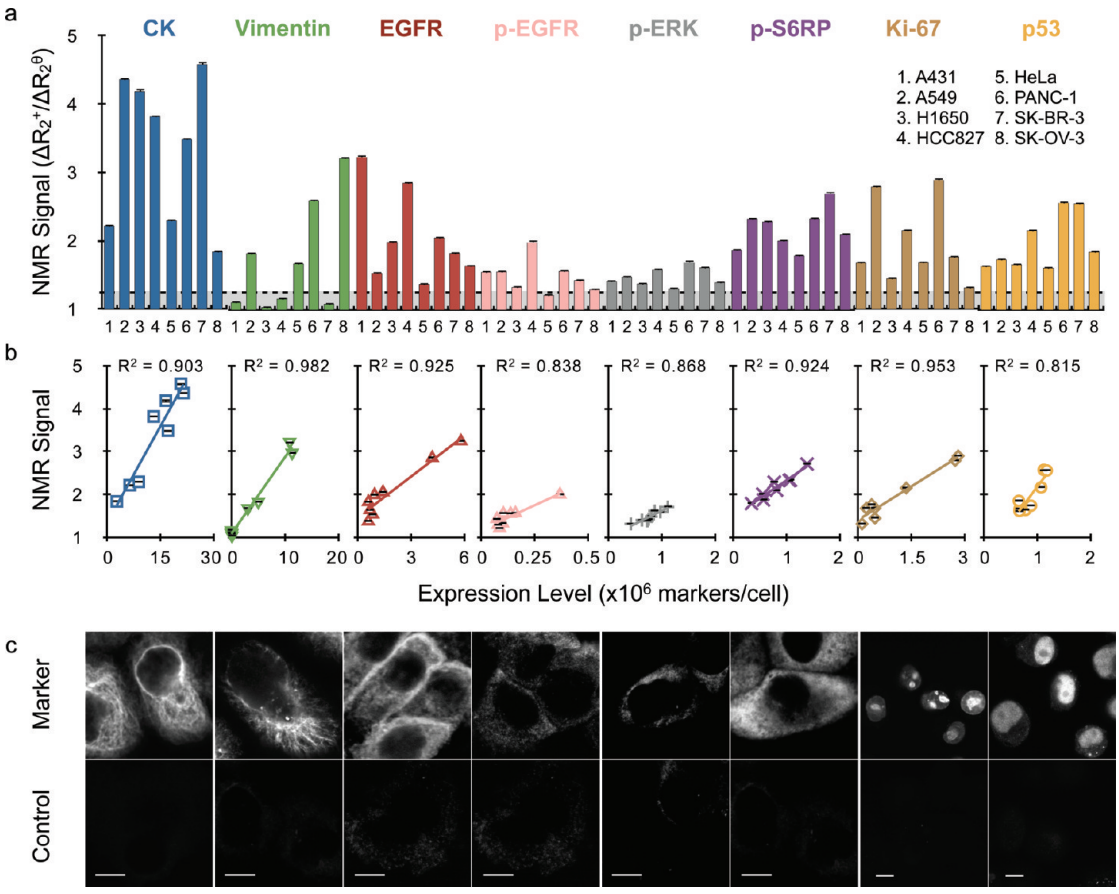

Figure 3. Profiling scant tumor cell populations for key biomarkers of cancer using diagnostic magnetic resonance (DMR). (a) Detection of eight biomarkers in eight different cell lines using MFNP based on nuclear magnetic resonance signal. The transverse relaxation rate (R_2) was measured for ~1000 cells using a miniaturized DMR device. Marker expression levels were determined based on the ratio of the positive marker (ΔR_2^{+}) and control (ΔR_2^{θ}) signals (see Methods). (b) Magnetic measurements showed excellent correlation with marker expression levels determined independently by antibody staining (see Supporting Information Table S2). (d) Confocal images demonstrating varying cellular localizations and signal intensities obtained for each specific marker (top) and controls (bottom). PANC-1 cells were used for CK, vimentin, p-ERK, p-S6RP, K_i-67, and p53 images. A431 cells were used for both EGFR cases. All scale bars represent 10 μm. Error bars represent the standard error from at least three μNMR measurements. Abbreviations: p-, phosphorylation specific; S6RP, S6 ribosomal protein.

experiments (1000 cells) and the expression levels measured by fluorescent antibody staining in larger samples (10^6 cells; see Supporting Information and Table S2). Confocal images in Figure 3c demonstrate the varying MFNP localizations and signal intensities obtained for each marker in PANC-1 (CK, vimentin, p-ERK, p-S6RP, K_i-67, and p53) and A431 (EGFR and p-EGFR) cells. Control signals were determined using a TCO-modified control antibody. These data show that DMR can be used to sense magnetic nanoparticles that are targeted to diverse proteins, including low-expression level phospho-proteins, in various intracellular locations and in scant cell samples.

Measuring Drug Efficacy. A transformational application of the DMR technology would be to quantitate drug efficacy in small tumor cell populations. The ability to measure drug effects on intracellular signaling pathways in target cells would have far reaching applications in pharmaceutical development and for routine clinical practice. Therefore, we assessed the activation state of cancer cells that were treated with inhibitors of the EGFR (gefitinib) and mTOR (rapamycin) signaling pathways by measuring the shared downstream target p-S6RP (Figure 4a). Administration of gefitinib to A431 (highly sensitive due to EGFR amplification), NCI-H1650 (moderately sensitive due to exon 19 deletion of EGFR), and A549 (not sensitive due to KRAS mutation) cells resulted in dose-dependent inhibition of p-S6RP that could accurately be quantitated in ~1000 cells by DMR (Figure 4b, c). IC_{50} values were approximately 10 nM for A431, 2 nM for NCI-H1650 (only 50% inhibition), and >10 μM for A549 cells, similar to previous reports.[37,38] Rapamycin IC_{50} values were approximately 0.5 nM for each cell line, similar to the subnanomolar (0.2 nM) binding constant reported.[39]

Application to Quantum Dots. As a final demonstration of the general applicability of the methods developed here, we tested commercially available quantum dots (QDs). QDs are ideal for fluorescence imaging applications due to their unique spectral properties, including signal strength, photostability, and narrow emission

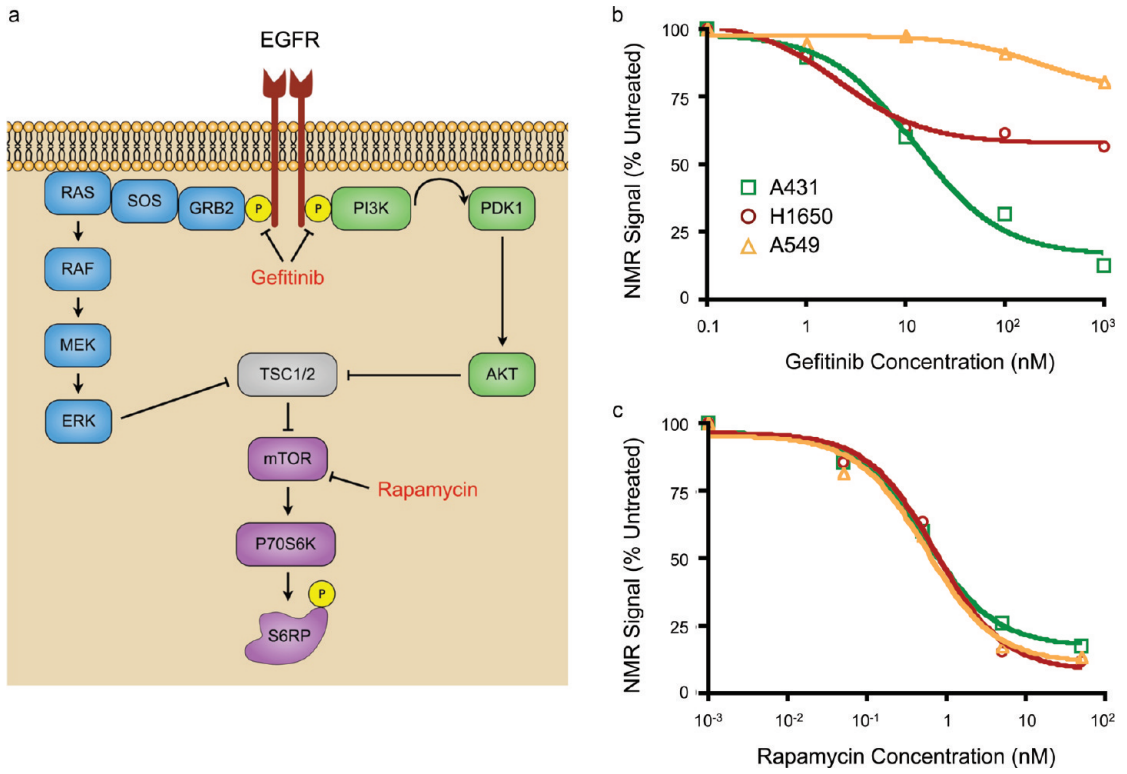

Figure 4. Therapeutic effects can be monitored using DMR on scant cell populations. (a) Gefitinib inhibits signaling *via* EGFR, ultimately leading to inhibition of the mTOR pathway and decreased cell growth. Rapamycin is a direct inhibitor of mTOR, leading to similar effects. (b,c) Three cell lines (A431, NCI-H1650, and A549) were treated with varying doses of gefitinib (1 to 1000 nM) or rapamycin (0.05 to 50 nM) for 12 h, and p-S6RP was used as a read-out of drug efficacy. (b) A431 and NCI-H1650 cell lines were highly sensitive to gefitinib, although the latter was only inhibited by 50%, and A549 cells were resistant. (d) Rapamycin inhibited all cell lines equally. Error bars represent the standard error from at least three μNMR measurements.

profiles.[7−9] Amine-terminated, PEG-coated QDs were modified with Tz (Tz-QD) and targeted to CK and K_i-67 in PANC-1 cells as described previously for Tz-MFNP. As the confocal microscopy images in Figure 5 illustrate, strong QD signals were obtained that spatially correlated with the targeting antibody. Signal-to-background ratios were lower than observed for MFNP, however, resulting in dim QD signal outside of the target area. This finding may have resulted from lower Tz valency, leading to less efficient binding, or instability of the proprietary PEG coating, causing higher background. The latter factor could likely be improved through use of more stable polymer coatings.[40] These results confirm that the cell treatments and BOND-2 targeting scheme are broadly applicable to different nanomaterials.

DISCUSSION

Our results demonstrate that we have improved nanoparticle targeting to cytoplasmic and nuclear proteins in comparison to traditional direct immunoconjugation, and thereby significantly increased the detection sensitivity and specificity of nanomaterial sensors. This was made possible by employing an advanced labeling scheme that uses bioorthogonal chemistry to amplify nanoparticle binding (BOND-2). Furthermore, we have maximized the potential of BOND by optimizing semipermeabilization of cells without cellular destruction. Our results show broad applicability and remarkable reproducibility across a platform of different intracellular biomarkers of diagnostic interest. This nanomaterial targeting technique is also sensitive, rapid, scalable, and adaptable to numerous types of nanomaterials. We envision that the described technique will facilitate a number of sensing applications under different detection modalities.

In the described work, we demonstrated improved targeting of nanomaterial sensors possessing fluorescent and magnetic properties. For magnetic nanoparticles, miniaturized NMR readers have recently been developed for *ex vivo* profiling of cancer cells in biological specimens.[14,41] These systems were previously limited to extracellular biomarkers,[14] but the techniques developed here will increase the number and type of biomarker targets available to nanomaterials for sensitive molecular detection (*i.e.*, CK or PSA for circulating tumor cells[42−46]) and comprehensive profiling, while also enabling real-time monitoring of therapeutic treatment efficacy (*i.e.*, p-S6RP). Given the high signal intensity and photostability of QDs, these techniques will also improve the sensitivity of intracellular protein detection

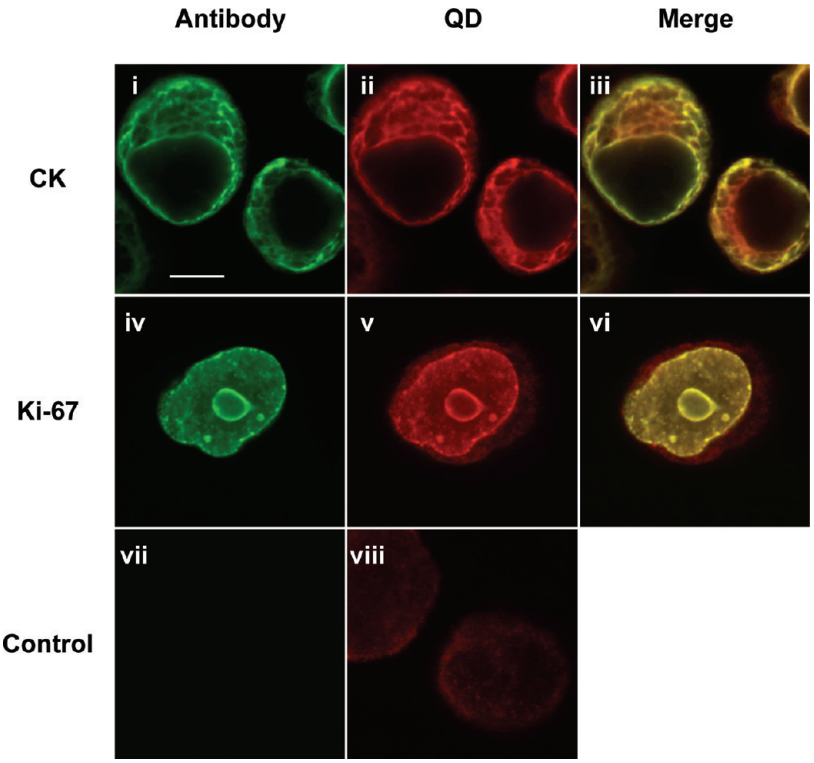

Figure 5. Quantum dots (QDs) can be targeted with high specificity using the described techniques. The Tz-QDs were targeted to PANC-1 cells labeled with TCO-modified, AF488 fluorescent antibodies to CK and K_i-67 as in Figure 2. Merged images demonstrate strong colocalization between the positive signals, confirming that QDs are targeted with high specificity to the intended target. The scale bar in (i) represents 10 μm.

in fluorescence imaging applications, potentially revealing the spatial localization of scant or even single molecular species. These benefits would extend to both discrete cell populations and tissue sections,[23−26] and multicolor fluorescence detection may be possible if used in concert with traditional affinity molecule−nanoparticle conjugates or a platform of appropriate bioorthogonal chemistries. While not demonstrated here, we envision that similar results could be obtained for gold and other nanoparticles for detection by SERS and electron microscopy.

The techniques described may also make it possible to directly monitor the delivery of small-molecule therapeutics (*i.e.*, TCO-modified drugs[36]) with nanomaterials, as well as impact biomedical applications such as magnetic cell separation based on intracellular targets and SILAC-based proteomic analysis.[47] Finally, while not specifically investigated here, it may be feasible to utilize reversible permeabilization methods (*e.g.*, streptolysin O[48]) to access intracellular proteins in viable cells for molecular sensing, cell tracking,[49,50] magneto-fection[51] and magnetic field-assisted drug delivery[21] and release[52] applications.

METHODS

Preparation of Tetrazine-Modified Nanoparticles. Magneto-fluorescent nanoparticles (MFNP) containing primary amine functional groups were prepared by synthesizing cross-linked iron oxide (CLIO) magnetic nanoparticles and reacting with a limited quantity of amine-reactive cyanine dye (VivoTag 680, VT680, VisEn Biomedical), as described elsewhere.[13] The amino-MFNP contained approximately 84 primary amine and 4.7 VT680 molecules per particle as determined by *N*-succinimidyl-3-(2-pyridyldithio)propionate (SPDP; Thermo Fisher)/dithiothreitol reaction[53] and absorbance measurement, respectively. The hydrodynamic diameter was 28.8 nm by dynamic light scattering (Zetasizer 1000HS; Malvern Instruments), and the r_1 and r_2 relaxivities were 25.2 and 64.5 mM^{-1} s^{-1}, respectively, at 40 °C and 0.47 T (Minispec MQ20; Bruker). Quantum dots with fluorescence emission maximum at 705 nm (Qdot 705) and an amine-derivatized PEG coating were purchased from Invitrogen and used directly. Amine-terminated nanoparticles were modified with 2,5-dioxopyrrolidin-1-yl 5-(4-(1,2,4,5-tetrazin-3-yl) benzylamino)-5-oxopentanoate (Tz-NHS) that was synthesized as previously reported[13] to create Tz nanoparticles. This reaction was performed using 500 equivalents of Tz-NHS relative to the molar concentration of nanoparticles and was performed in PBS containing 5% dimethylformamide (DMF) for 3 h at room temperature. Excess Tz-NHS was removed by gel filtration using Sephadex G-50 (GE Healthcare), and concentration was determined by absorbance measurement at 410 nm (MFNP) or fluorescence intensity (QD) relative to stock samples. MFNP mass concentration was converted to molar concentration using an estimated 447 000 Da molecular weight for CLIO (8000 Fe atoms per core crystal, 55.85 Da each[54]).

Preparation of TCO-Modified Antibodies. Monoclonal antibodies were modified with (*E*)-cyclooct-4-enyl-2,5-dioxopyrrolidin-1-yl carbonate (TCO-NHS) that was synthesized as previously reported.[35] If present, sodium azide was first removed by buffer

exchange into PBS (pH 8.0) using a 2 mL Zeba desalting column (Thermo Fisher). TCO-NHS was then reacted with 0.5 mg of antibody in 10% DMF for 3 h at room temperature. The antipan cytokeratin antibody (clone C-11, EXBIO) was reacted with 10, 100, and 1000 equiv of TCO-NHS. All of the other antibodies (listed in Supporting Information Table S1) were reacted with 1000 equiv only. Samples were purified using Zeba columns, and mass concentrations were determined by absorbance measurement. TCO valencies were determined based on changes in molecular weight using MALDI-TOF (matrix-assisted laser desorption/ionization time-of-flight) mass spectrometry (see Supporting Information). Antibody-MFNP immuno-conjugates were prepared from TCO-antibody and Tz-MFNP (see Supporting Information).

Cell Fixation and Permeabilization Treatments. The human cancer cell lines SK-BR-3, PANC-1, HeLa, SK-OV-3, U118, HT-29, A549, A431, and HCC827 were obtained from ATCC and maintained in DMEM media supplemented with 10% fetal bovine serum (FBS) and 5% penicillin/streptomycin. For drug inhibition studies, cells were treated with gefitinib (Thermo Fisher) at 1, 10, 100, or 1000 nM or rapamycin (Sigma Aldrich) at 0.05, 0.5, 5, or 50 nM in DMEM for 24 h. Prior to fixation, cells were grown to ~90% confluency, released using 0.05% Tryspin/0.53 mM EDTA, and washed twice by centrifugation with PBS containing 2% FBS (PBS+). In some cases, a freeze−thaw regimen was performed by suspending the cells in PBS+ containing 15% glycerol, rapidly freezing in a bath of dry ice and isopropyl alcohol, and thawing at 37 °C. Cells (5×10^6 per treatment) were fixed by suspending in a 1:1 mixture of PBS and Fix buffer 1 (FB1, BD Biosciences) and incubating at room temperature for 20 min. Cells comprising the non-treated (NT) subset were then washed three times with PBS+ and used directly. Additional permeabilization treatments were performed for the other cases by washing once with PBS+, incubating for 20 min in Tween 20 (Tw20; 1% in PBS, room temperature), Triton X-100 (TX; 0.05% in PBS, room temperature), or ice-cold methanol (Meth; 100%, on ice), and washing three times with PBS+. Finally, the additional saponin subset (Spn) was washed three times with perm/wash buffer containing 1% BSA (PW+, BD Biosciences). Since permeabilization with saponin is reversible, PW+ was employed for all subsequent cell treatments of the Spn subset.

Nanoparticle Targeting and Detection. Fixed and permeabilized cells (250 000/sample) were labeled with TCO-modified monoclonal antibody (10 μg/mL) in 0.15 mL of PBS+ or PW+ for 10 min at room temperature, pelleted by centrifugation, and aspirated. Tz-MFNP (0.2 to 200 nM) or Tz-QD (25 nM) was then added directly, and the sample was vortexed, incubated for 30 min at room temperature on a rotator, and washed twice by centrifugation with PBS+ or PW+. Antibodies were omitted for control samples. For direct labeling with immuno-MFNP conjugates, only the MFNP binding period (0.2 to 100 nM) was employed. Fluorescence intensity was assessed using an LSRII flow cytometer (Becton Dickinson), and mean fluorescence intensity was determined using FlowJo software. All measurements were performed in triplicate, and the data are presented as the mean ± standard error.

Magnetic resonance measurements were performed using a miniaturized nuclear magnetic resonance device.[13,14] Transverse relaxation rate (R_2) was measured for approximately 1000 cells within the 1 μL sample volume of the microcoil using Carr−Purcell−Meiboom−Gill pulse sequences with the following parameters: echo time (TE) = 4 ms; repetition time (TR) = 6 s; the number of 180° pulses per scan = 500; the number of scans = 8. All measurements were performed in triplicate, and the data are presented as mean ± standard error. The R_2 values were converted to the marker expression level per cell by subtracting the R_2 value for unlabeled cells to obtain ΔR_2 and dividing the marker specific ΔR_2 (ΔR_2^+) by the control (ΔR_2^0).[13,14]

For confocal microscopy studies, cells were grown on glass slides with removable chamber wells (Lab-Tek; Thermo Fisher). Cell labeling was performed as described above, and fluorescence signal was imaged using a multichannel upright laser-scanning confocal microscope (FV1000; Olympus) with a 60× water immersion objective lens. Images were acquired with Fluoview software (version 4.3; Olympus) and analyzed using ImageJ software (version 1.41; Bethesda, MD).

Acknowledgment. The authors thank N. Sergeyev for synthesizing CLIO, S. Hilderbrand for synthesizing the tetrazine precursor, and V. Peterson for assistance with cell culture. We also thank M. Pittet, F. Swirski, and Y. Fisher-Jeffes for many helpful discussions and critical review of the manuscript. This work was funded in part by NCI Grant P50CA86355. J.B.H. was supported in part by NCI fellowship F32CA144139, and N.K.D. was supported in part by NIBIB Grant K01EB010078. The following NIH funding sources are also acknowledged: U54 11934, U54 CA 151884, R01 EB 004626, R01 EB 010011 and HHSN268201000044C.

Supporting Information Available: Supporting methods outlining the measurement of TCO valency on monoclonal antibodies using MALDI-TOF, creation of MFNP immuno-conjugates, and measurement of cellular biomarker expression levels using flow cytometry. Supporting Figures S1 and S2 showing antibody-TCO MALDI-TOF data and MFNP targeting to vimentin and p53, and cytokeratin and vimentin Western blots. Supporting Tables S1 and S2 detailing information about monoclonal antibodies used in this study and cellular biomarker expression levels measured by flow cytometry. This material is available free of charge *via* the Internet at http://pubs.acs.org.

REFERENCES AND NOTES

1. Spencer, S. L.; Gaudet, S.; Albeck, J. G.; Burke, J. M.; Sorger, P. K. Non-genetic Origins of Cell-to-Cell Variability in TRAIL-Induced Apoptosis. *Nature* **2009,** *459*, 428–432.
2. Spiller, D. G.; Wood, C. D.; Rand, D. A.; White, M. R. Measurement of Single-Cell Dynamics. *Nature* **2010,** *465*, 736–745.
3. Hood, L.; Heath, J. R.; Phelps, M. E.; Lin, B. Systems Biology and New Technologies Enable Predictive and Preventative Medicine. *Science* **2004,** *306*, 640–643.
4. Dowsett, M.; Dunbier, A. K. Emerging Biomarkers and New Understanding of Traditional Markers in Personalized Therapy for Breast Cancer. *Clin. Cancer Res.* **2008,** *14*, 8019–8026.
5. Haun, J. B.; Yoon, T. J.; Lee, H.; Weissleder, R. Magnetic Nanoparticle Biosensors. *Wiley Interdiscip. Rev. Nanomed. Nanobiotechnol.* **2010,** *2*, 291–304.
6. Lee, J. H.; Huh, Y. M.; Jun, Y. W.; Seo, J. W.; Jang, J. T.; Song, H. T.; Kim, S.; Cho, E. J.; Yoon, H. G.; Suh, J. S.; Cheon, J. Artificially Engineered Magnetic Nanoparticles for Ultra-sensitive Molecular Imaging. *Nat. Med.* **2007,** *13*, 95–99.
7. Alivisatos, P. The Use of Nanocrystals in Biological Detection. *Nat. Biotechnol.* **2004,** *22*, 47–52.
8. Michalet, X.; Pinaud, F. F.; Bentolila, L. A.; Tsay, J. M.; Doose, S.; Li, J. J.; Sundaresan, G.; Wu, A. M.; Gambhir, S. S.; Weiss, S. Quantum Dots for Live Cells, *In Vivo* Imaging, and Diagnostics. *Science* **2005,** *307*, 538–544.
9. Medintz, I. L.; Uyeda, H. T.; Goldman, E. R.; Mattoussi, H. Quantum Dot Bioconjugates for Imaging, Labelling and Sensing. *Nat. Mater.* **2005,** *4*, 435–446.
10. Hilderbrand, S. A.; Shao, F.; Salthouse, C.; Mahmood, U.; Weissleder, R. Upconverting Luminescent Nanomaterials: Application to *In Vivo* Bioimaging. *Chem. Commun.* **2009,** 4188–4190.
11. Wang, F.; Liu, X. Recent Advances in the Chemistry of Lanthanide-Doped Upconversion Nanocrystals. *Chem. Soc. Rev.* **2009,** *38*, 976–989.
12. Anker, J. N.; Hall, W. P.; Lyandres, O.; Shah, N. C.; Zhao, J.; Van Duyne, R. P. Biosensing with Plasmonic Nanosensors. *Nat. Mater.* **2008,** *7*, 442–453.
13. Haun, J. B.; Devaraj, N. K.; Hilderbrand, S. A.; Lee, H.; Weissleder, R. Bioorthogonal Chemistry Amplifies Nanoparticle Binding and Enhances the Sensitivity of Cell Detection. *Nat. Nanotechnol.* **2010,** *5*, 660–665.
14. Lee, H.; Yoon, T. J.; Figueiredo, J. L.; Swirski, F. K.; Weissleder, R. Rapid Detection and Profiling of Cancer Cells in Fine-Needle Aspirates. *Proc. Natl. Acad. Sci. U.S.A.* **2009,** *106*, 12459–12464.
15. Jaiswal, J. K.; Mattoussi, H.; Mauro, J. M.; Simon, S. M. Long-Term Multiple Color Imaging of Live Cells Using Quantum Dot Bioconjugates. *Nat. Biotechnol.* **2003,** *21*, 47–51.

16. Gao, X.; Cui, Y.; Levenson, R. M.; Chung, L. W.; Nie, S. *In Vivo* Cancer Targeting and Imaging with Semiconductor Quantum Dots. *Nat. Biotechnol.* **2004,** *22*, 969–976.
17. Nyk, M.; Kumar, R.; Ohulchanskyy, T. Y.; Bergey, E. J.; Prasad, P. N. High Contrast *In Vitro* and *In Vivo* Photoluminescence Bioimaging Using Near Infrared to Near Infrared Up-Conversion in Tm^{3+} and Yb^{3+} Doped Fluoride Nanophosphors. *Nano Lett.* **2008,** *8*, 3834–3838.
18. Wang, M.; Mi, C. C.; Wang, W. X.; Liu, C. H.; Wu, Y. F.; Xu, Z. R.; Mao, C. B.; Xu, S. K. Immunolabeling and NIR-Excited Fluorescent Imaging of HeLa Cells By Using NaYF(4):Yb,Er Upconversion Nanoparticles. *ACS Nano* **2009,** *3*, 1580–1586.
19. Wu, S.; Han, G.; Milliron, D. J.; Aloni, S.; Altoe, V.; Talapin, D. V.; Cohen, B. E.; Schuck, P. J. Non-blinking and Photostable Upconverted Luminescence From Single Lanthanide-Doped Nanocrystals. *Proc. Natl. Acad. Sci. U.S.A.* **2009,** *106*, 10917–10921.
20. Qian, X.; Peng, X. H.; Ansari, D. O.; Yin-Goen, Q.; Chen, G. Z.; Shin, D. M.; Yang, L.; Young, A. N.; Wang, M. D.; Nie, S. *In Vivo* Tumor Targeting and Spectroscopic Detection with Surface-Enhanced Raman Nanoparticle Tags. *Nat. Biotechnol.* **2008,** *26*, 83–90.
21. Liu, Z.; Li, X.; Tabakman, S. M.; Jiang, K.; Fan, S.; Dai, H. Multiplexed Multicolor Raman Imaging of Live Cells with Isotopically Modified Single Walled Carbon Nanotubes. *J. Am. Chem. Soc.* **2008,** *130*, 13540–13541.
22. Wu, X.; Liu, H.; Liu, J.; Haley, K. N.; Treadway, J. A.; Larson, J. P.; Ge, N.; Peale, F.; Bruchez, M. P. Immunofluorescent Labeling of Cancer Marker Her2 and Other Cellular Targets with Semiconductor Quantum Dots. *Nat. Biotechnol.* **2003,** *21*, 41–46.
23. Ghazani, A. A.; Lee, J. A.; Klostranec, J.; Xiang, Q.; Dacosta, R. S.; Wilson, B. C.; Tsao, M. S.; Chan, W. C. High Throughput Quantification of Protein Expression of Cancer Antigens in Tissue Microarray Using Quantum Dot Nanocrystals. *Nano Lett.* **2006,** *6*, 2881–2886.
24. Yezhelyev, M. V.; Al-Hajj, A.; Morris, C.; Marcus, A. I.; Liu, T.; Lewis, M.; Cohen, C.; Zrazhevskiy, P.; Simons, J. W.; Rogatko, A. *In Situ* Molecular Profiling of Breast Cancer Biomarkers with Multicolor Quantum Dots. *Adv. Mater.* **2007,** *19*, 3146–3151.
25. Bodo, J.; Durkin, L.; Hsi, E. D. Quantitative *In Situ* Detection of Phosphoproteins in Fixed Tissues Using Quantum Dot Technology. *J. Histochem. Cytochem.* **2009,** *57*, 701–708.
26. Liu, J.; Lau, S. K.; Varma, V. A.; Moffitt, R. A.; Caldwell, M.; Liu, T.; Young, A. N.; Petros, J. A.; Osunkoya, A. O.; Krogstad, T.; *et al.* Molecular Mapping of Tumor Heterogeneity on Clinical Tissue Specimens with Multiplexed Quantum Dots. *ACS Nano* **2010,** *4*, 2755–2765.
27. Delehanty, J. B.; Mattoussi, H.; Medintz, I. L. Delivering Quantum Dots into Cells: Strategies, Progress and Remaining Issues. *Anal. Bioanal. Chem.* **2009,** *393*, 1091–1105.
28. Verma, A.; Stellacci, F. Effect of Surface Properties on Nanoparticle−Cell Interactions. *Small* **2010,** *6*, 12–21.
29. Petros, R. A.; DeSimone, J. M. Strategies in the Design of Nanoparticles for Therapeutic Applications. *Nat. Rev. Drug Discovery* **2010,** *9*, 615–627.
30. Lewin, M.; Carlesso, N.; Tung, C. H.; Tang, X. W.; Cory, D.; Scadden, D. T.; Weissleder, R. Tat Peptide-Derivatized Magnetic Nanoparticles Allow *In Vivo* Tracking and Recovery of Progenitor Cells. *Nat. Biotechnol.* **2000,** *18*, 410–414.
31. Ruan, G.; Agrawal, A.; Marcus, A. I.; Nie, S. Imaging and Tracking of Tat Peptide-Conjugated Quantum Dots in Living Cells: New Insights into Nanoparticle Uptake, Intracellular Transport, and Vesicle Shedding. *J. Am. Chem. Soc.* **2007,** *129*, 14759–14766.
32. Delehanty, J. B.; Bradburne, C. E.; Boeneman, K.; Susumu, K.; Farrell, D.; Mei, B. C.; Blanco-Canosa, J. B.; Dawson, G.; Dawson, P. E.; Mattoussi, H.; Medintz, I. L. Delivering Quantum Dot-Peptide Bioconjugates to the Cellular Cytosol: Escaping from the Endolysosomal System. *Integr. Biol.* **2010,** *2*, 265–277.
33. Han, H. S.; Devaraj, N. K.; Lee, J.; Hilderbrand, S. A.; Weissleder, R.; Bawendi, M. G. Development of a Bioorthogonal and Highly Efficient Conjugation Method for Quantum Dots Using Tetrazine−Norbornene Cycloaddition. *J. Am. Chem. Soc.* **2010,** *132*, 7838–7839.
34. Devaraj, N. K.; Weissleder, R.; Hilderbrand, S. A. Tetrazine-Based Cycloadditions: Application to Pretargeted Live Cell Imaging. *Bioconjugate Chem.* **2008,** *19*, 2297–2299.
35. Devaraj, N. K.; Upadhyay, R.; Haun, J. B.; Hilderbrand, S. A.; Weissleder, R. Fast and Sensitive Pretargeted Labeling of Cancer Cells through a Tetrazine/*trans*-Cyclooctene Cycloaddition. *Angew. Chem., Int. Ed.* **2009,** *48*, 7013–7016.
36. Devaraj, N. K.; Hilderbrand, S.; Upadhyay, R.; Mazitschek, R.; Weissleder, R. Bioorthogonal Turn-On Probes for Imaging Small Molecules Inside Living Cells. *Angew. Chem., Int. Ed.* **2010,** *49*, 2869–2872.
37. Helfrich, B. A.; Raben, D.; Varella-Garcia, M.; Gustafson, D.; Chan, D. C.; Bemis, L.; Coldren, C.; Baron, A.; Zeng, C.; Franklin, W. A.; *et al.* Antitumor Activity of the Epidermal Growth Factor Receptor (EGFR) Tyrosine Kinase Inhibitor Gefitinib (ZD1839, Iressa) in Non-Small Cell Lung Cancer Cell Lines Correlates with Gene Copy Number and EGFR Mutations but Not EGFR Protein Levels. *Clin. Cancer Res.* **2006,** *12*, 7117–7125.
38. Guix, M.; Faber, A. C.; Wang, S. E.; Olivares, M. G.; Song, Y.; Qu, S.; Rinehart, C.; Seidel, B.; Yee, D.; Arteaga, C. L.; Engelman, J. A. Acquired Resistance to EGFR Tyrosine Kinase Inhibitors in Cancer Cells is Mediated by Loss of IGF-Binding Proteins. *J. Clin. Invest.* **2008,** *118*, 2609–2619.
39. Schreiber, S. L. Chemistry and Biology of the Immunophilins and Their Immunosuppressive Ligands. *Science* **1991,** *251*, 283–287.
40. Liu, W.; Greytak, A. B.; Lee, J.; Wong, C. R.; Park, J.; Marshall, L. F.; Jiang, W.; Curtin, P. N.; Ting, A. Y.; Nocera, D. G.; *et al.* Compact Biocompatible Quantum Dots *via* RAFT-Mediated Synthesis of Imidazole-Based Random Copolymer Ligand. *J. Am. Chem. Soc.* **2010,** *132*, 472–483.
41. Lee, H.; Sun, E.; Ham, D.; Weissleder, R. Chip-NMR Biosensor for Detection and Molecular Analysis of Cells. *Nat. Med.* **2008,** *14*, 869–874.
42. Allard, W. J.; Matera, J.; Miller, M. C.; Repollet, M.; Connelly, M. C.; Rao, C.; Tibbe, A. G.; Uhr, J. W.; Terstappen, L. W. Tumor Cells Circulate in the Peripheral Blood of All Major Carcinomas but Not in Healthy Subjects or Patients with Nonmalignant Diseases. *Clin. Cancer Res.* **2004,** *10*, 6897–6904.
43. Cristofanilli, M.; Budd, G. T.; Ellis, M. J.; Stopeck, A.; Matera, J.; Miller, M. C.; Reuben, J. M.; Doyle, G. V.; Allard, W. J.; Terstappen, L. W.; Hayes, D. F. Circulating Tumor Cells, Disease Progression, and Survival in Metastatic Breast Cancer. *N. Engl. J. Med.* **2004,** *351*, 781–791.
44. Nagrath, S.; Sequist, L. V.; Maheswaran, S.; Bell, D. W.; Irimia, D.; Ulkus, L.; Smith, M. R.; Kwak, E. L.; Digumarthy, S.; Muzikansky, A.; *et al.* Isolation of Rare Circulating Tumour Cells in Cancer Patients by Microchip Technology. *Nature* **2007,** *450*, 1235–1239.
45. Maheswaran, S.; Sequist, L. V.; Nagrath, S.; Ulkus, L.; Brannigan, B.; Collura, C. V.; Inserra, E.; Diederichs, S.; Iafrate, A. J.; Bell, D. W.; *et al.* Detection of Mutations in EGFR in Circulating Lung-Cancer Cells. *N. Engl. J. Med.* **2008,** *359*, 366–377.
46. Stott, S. L.; Lee, R. J.; Nagrath, S.; Yu, M.; Miyamoto, D. T.; Ulkus, L.; Inserra, E. J.; Ulman, M.; Springer, S.; Nakamura, Z.; *et al.* Isolation and Characterization of Circulating Tumor Cells from Patients with Localized and Metastatic Prostate Cancer. *Sci. Transl. Med.* **2010,** *2*, 25ra23.
47. Ong, S. E.; Blagoev, B.; Kratchmarova, I.; Kristensen, D. B.; Steen, H.; Pandey, A.; Mann, M. Stable Isotope Labeling by Amino Acids in Cell Culture, SILAC, as a Simple and Accurate Approach to Expression Proteomics. *Mol. Cell Proteomics* **2002,** *1*, 376–386.
48. Ahnert-Hilger, G.; Bader, M. F.; Bhakdi, S.; Gratzl, M. Introduction of Macromolecules into Bovine Adrenal Medullary Chromaffin Cells and Rat Pheochromocytoma Cells (PC12) by Permeabilization with Streptolysin O: Inhibitory Effect of Tetanus Toxin on Catecholamine Secretion. *J. Neurochem.* **1989,** *52*, 1751–1758.

49. Voura, E. B.; Jaiswal, J. K.; Mattoussi, H.; Simon, S. M. Tracking Metastatic Tumor Cell Extravasation with Quantum Dot Nanocrystals and Fluorescence Emission-Scanning Microscopy. *Nat. Med.* **2004,** *10*, 993–998.
50. Stroh, M.; Zimmer, J. P.; Duda, D. G.; Levchenko, T. S.; Cohen, K. S.; Brown, E. B.; Scadden, D. T.; Torchilin, V. P.; Bawendi, M. G.; Fukumura, D.; Jain, R. K. Quantum Dots Spectrally Distinguish Multiple Species within the Tumor Milieu *In Vivo*. *Nat. Med.* **2005,** *11*, 678–682.
51. Scherer, F.; Anton, M.; Schillinger, U.; Henke, J.; Bergemann, C.; Kruger, A.; Gansbacher, B.; Plank, C. Magnetofection: Enhancing and Targeting Gene Delivery By Magnetic Force *In Vitro* and *In Vivo*. *Gene Ther.* **2002,** *9*, 102–109.
52. Giri, S.; Trewyn, B. G.; Stellmaker, M. P.; Lin, V. S. Stimuli-Responsive Controlled-Release Delivery System Based on Mesoporous Silica Nanorods Capped with Magnetic Nanoparticles. *Angew. Chem., Int. Ed.* **2005,** *44*, 5038–5044.
53. Zhao, M.; Kircher, M. F.; Josephson, L.; Weissleder, R. Differential Conjugation of Tat Peptide to Superparamagnetic Nanoparticles and Its Effect on Cellular Uptake. *Bioconjugate Chem.* **2002,** *13*, 840–844.
54. Reynolds, F.; O'loughlin, T.; Weissleder, R.; Josephson, L. Method of Determining Nanoparticle Core Weight. *Anal. Chem.* **2005,** *77*, 814–817.